a pressure vs time trace based on the known low-pressure data. The grain is fired normally and the pressure vs time trace is reduced for a given number of time increments and the pressures obtained at these increments are used as input to the computer program. The actual pressure vs time trace is replotted by the computer to the same time base as the original theoretical trace. The comparison of the two traces then defines the point of instability if it exists in the pressure region investigated (Fig. 5).

Results

Epoxy/ammonium nitrate propellants exhibited stable burning up to 12,000 psi. Modification of particle size distribution, plasticizer, or replacement of up to 30% of the nitrate with ammonium perchlorate had no effect on the stability limit.

Gum rubber/ammonium nitrate propellants generally demonstrate stable burning up to 10,000 psi. Inclusion of burning rate catalyst content of 4% reduces critical pressure to 4700 psi. Oxidizer loading and plasticizer content had no significant effect. Replacement of the nitrate with ammonium perchlorate resulted in a critical pressure of 3600 psi.

Polysulfide/ammonium perchlorate propellants are stable to the 5000–6000 psi range. Increases of burning rate catalyst and fine oxidizer content tends to decrease stability. Plasticizer or aluminum content, in quantities of two to three percent are not significant to stability.

Polyvinyl chloride/ammonium perchlorate propellants tend to greater stability with lower oxidizer content, in these cases the more stable formulation contains only fine oxidizer.

Polybutadiene/ammonium perchlorate propellants exhibit unstable burning from 3400 to 7000 psi dependent upon formulations. The least stable system contains random-terminated polymer, an intermediate is a saturated hydrocarbon, and the most stable system is the carboxy-terminated polymer. Generally, for the carboxy-terminated polymer, as solids and plasticizer content increase so does the critical pressure. Oxidizer particle size distribution appears to have no effect on the pressure stability of the propellant. Replacement of perchlorate with ammonium nitrate tends to increase the critical pressure.

Crew Locomotion Disturbances in a Space Cabin Simulator

M. Goodman* and W. C. Middleton†
McDonnell Douglas Astronautics Company, Santa Monica, Calif.

Introduction

Over the long run, crew locomotion disturbances to a space vehicle may be essentially cancelled out by return trips between stations in the vehicle. However, appreciable attitude errors can develop prior to this cancellation. Thus, it will be necessary to counteract these disturbances continuously as they occur by means of control torques generated by control moment gyros (CMGs), reaction control thrusters, or combinations of both. In the latter case, the thrusters are used to desaturate the CMG and to provide the simultaneous stationkeeping functions.

The magnitude of disturbance and net impulse imparted per event have been determined for three types of locomotion:

Received June 20, 1969; revision received July 31, 1969.

* Senior Engineer Scientist, Western Division. Associate Fellow AIAA.

† Senior Engineer Scientist, Western Division.

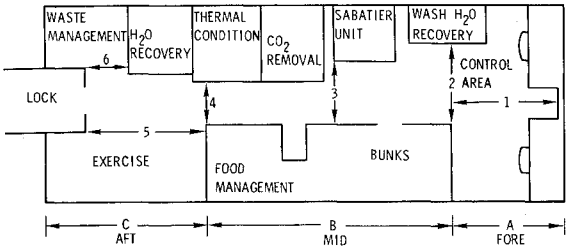

Fig. 1 Location of photoelectric light beams in the SCS.

free soaring, velcro walking, and hand rail walking, while the test subject was suspended to simulate the zero-gravity environment of a space vehicle.[1] However, little information has been available for predicting the frequency of locomotion to be expected within a space vehicle. An opportunity to obtain data on crew locomotion became available during an extended test of a life support system in the MDAC Space Cabin Simulator (SCS).[2] This Note presents some data on the locomotion of four crewmen during six separate 24-hr periods of a 60-day continuous test in the SCS. Six photoelectric relays and their associated light sources were installed within the SCS for this purpose (see numbers 1–6 and their light paths in Fig. 1). When a light beam was interrupted, one of six pens in an event recorder was activated. The cylindrical SCS, 12 ft in diameter and 40 ft long, contained the basic components of a life support system and hence simulated the geometry of a typical space station.

Test Results

The results of the crew travel studies were reported with the SCS arbitrarily divided into three general areas: 1) the forward command area, 2) the midgalley area, and 3) the aft waste management and exercise area. The crewmen spent considerably more time in the command area, which was the focal point in the SCS; most crew travel began and terminated in this area. Table 1 shows the round-trip travel between the three areas during each of the six 24-hr periods that were monitored. Travel on Sunday was obviously less than travel during the week days. This was expected because of the greater activity outside of the SCS on week days. There was no significant change in the amount of travel as the run progressed. For example, the same number of round trips were made on Tuesday, February 27, 1968 and on Tuesday, April 9, 42 days later. During the latter part of the 60-day run, there was an increase in the percentage of the day's travel activity that occurred between the command station and the galley, and less activity occurred in the vicinity of the exercise area.

Figure 2 shows the total activity as evidenced by photocell activations recorded within the SCS from 8:00 AM, Sunday, April 7, 1968 to 8:00 AM, Monday. This includes activity within each area and travel between the areas. These data are presented for a Sunday because the crewmen received fewer extraneous inputs from outside of the SCS on this day. The sharp peak in activity at midnight was caused by one crewman who paced back and forth each night as part of his

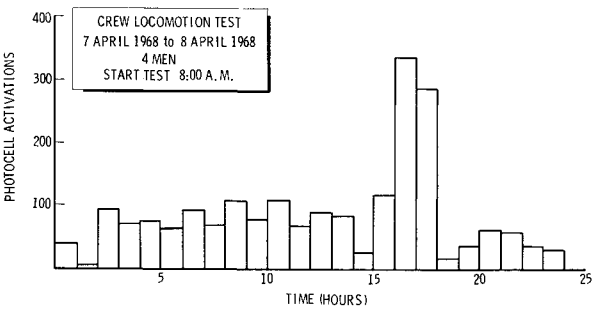

Fig. 2 Photocell activations vs time.

Table 1 Crew travel in the SCS

Round trips between	Feb. 27 (Tues.)	March 7 (Thurs.)	March 23 (Sun.)	April 7 (Sun.)	April 9 (Tues.)	April 16 (Tues.)
Command station and galley	192 (61%)[a]	133 (62%)	126 (63%)	116 (72%)	238 (76%)	194 (71%)
Command station and exercise and waste management area	44 (14%)	32 (15%)	33 (17%)	16 (10%)	26 (8%)	32 (12%)
Galley and exercise and waste management area	78 (25%)	48 (23%)	39 (20%)	29 (18%)	50 (16%)	46 (17%)
Total	314	213	198	161	314	272

[a] Note: Indicates the percent of the total travel activity for that day.

exercise program. His pacing was extremely uniform, both within each nightly period and from night to night.

Figure 3 is the one-way trips for the same period. The data were obtained by properly interpreting from the tapes (not shown) the successive interruption of photocells; for example, a trip from A to B (AB) required the activation of photocell 2 of Fig. 1, whereas a trip AC required the successive activations of photocells 2, 3, and 4. The rate of single trips taken reached a maximum of 30 per hour; the cumulative one-way trips on that day totaled 324 at an average of 13.5 per hour.

Disturbance to Vehicle

The one-way trips of Fig. 3 do not all result in a net displacement of the vehicle since, as previously mentioned, these include round trips that tend to cancel out the disturbances over a long period of time. Consequently, the data of Fig. 3 were evaluated over 10-min intervals, and a weighted relative disturbance factor δ was arbitrarily assigned to each type of trip as shown in Table 2. A positive sign indicated travel toward the aft direction and vice versa, and δ was assumed to increase with the length of travel distance between stations. This would appear to be a reasonably valid assumption since the longer the distance traveled, the more often contact and hence impulses would be applied to the vehicle; also the differences in moment arm (from the vehicle CG) and hence net torques would be larger with increasing distance between stations. On this basis the histogram of Fig. 4 resulted, taking into account both positive and negative trips. An unchanged disturbance level over a 10-min period indicated 1) either that no net travel had occurred between stations or 2) that positive and negative trips cancelled out.

The histogram of Fig. 4 gives only the relative magnitude and frequency of disturbance to the space vehicle. To determine the magnitude in terms of force or impulse (lb-sec) equivalent to δ, one must make an assumption with regard to the mode of locomotion, in this case free soaring. Under this mode of locomotion the astronaut pushes off and imparts a finite impulse to the support surface (say the floor of the vehicle). If the action takes place perpendicular to the axis at a distance from the vehicle c.g., the torque produced by the impulse causes the vehicle to accelerate to a fixed angular velocity during the short interval of time associated with the application of force. Next follows an interval of free soaring by the astronaut during which the vehicle continues to rotate at the fixed angular velocity. When the astronaut contacts the opposite vehicle surface and halts his flight, it is assumed that he imparts an impulse of equal magnitude but opposite sign to the rotating vehicle. The opposite torque applied over this short interval produces a negative acceleration and the vehicle's angular velocity is reduced to zero. The result is a net angular displacement of the vehicle from its original rest position. Reference 1 showed that a 36-lb-sec impulse was imparted to the vehicle at pushoff over a 0.35-sec duration. (The same magnitude of impulse is also assumed for impact.) If this action takes place at 20 ft from the c.g. of a space station having a 500,000 slug-ft^2 pitch moment of inertia as with the MORL (manned orbital research laboratory), then a 0.26° net displacement results. If this magnitude of disturbance level or displacement is then equated to the longest trip AC of Fig. 1, then $3\delta = 0.26°$ and $\delta = 0.09°$. Thus it can be seen from Fig. 4 that a maximum displacement of -5δ or $-0.45°$ occurs between the fifth and sixth hour. The mission requirements would indicate whether or not such a displacement is acceptable. The MORL, for example, has an attitude hold accuracy of $\pm 0.1°$ for certain of the precision experiments; hence an attitude control system of sufficient capacity would have to be exercised to counteract this disturbance displacement.

Conclusions

The data generated from the test showed that frequent crew motion in a space vehicle can produce control problems over extended time intervals during which extreme pointing accuracy is required. When realistic mission control requirements are known, data of this nature can be used to evaluate the attitude control system, and histograms similar to Fig. 4 may be used as inputs for crew locomotion disturbances in a vehicle control simulation computer program.

As far as this particular test is concerned, the authors recognize the limitations on the accuracy of data and resulting trip interpretations. For example, the test subject could

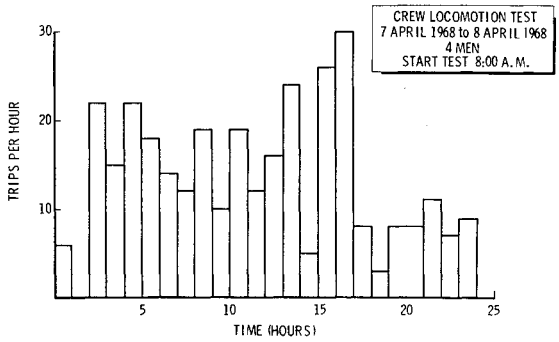

Fig. 3 One-way trips.

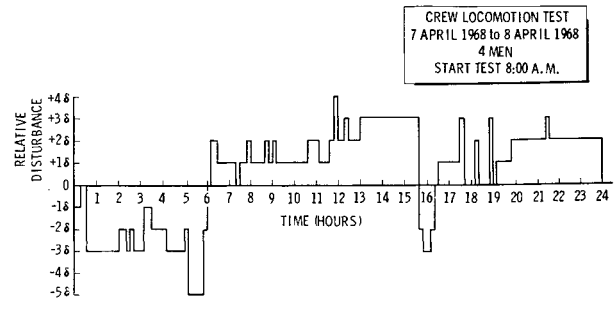

Fig. 4 Travel disturbance histogram.

Table 2 Weighted disturbance

Trip designation	Weighted value
AB, BA	$+1\delta$, -1δ, respectively
AC, CA	$+3\delta$, -3δ, respectively
BC, CB	$+2\delta$, -2δ, respectively

interrupt the photocell beam by hand waving or to and fro motion without actually taking a trip. Thus, improved techniques using a greater number of photocells and possibly incorporating television monitoring would help in upgrading the trip data resulting from future experiments.

References

[1] Fuhrmeister, W. F. and Fowler, J. L., "Experimental Study of Dynamic Effects of Crew Motion in a Manned Orbital Research Laboratory (MORL)," NASA CR-66186, Oct. 1966, McDonnell Douglas Astronautics Co., Western Div., Huntington Beach, Calif.

[2] Taliaferro, E. H. et al., "60-Day Manned Test of a Regenerative Life Support System with Oxygen and Water Recovery, Part II Aerospace Medicine and Man-Machine Test Results," NASA CR-98501, Dec. 1968, McDonnell Douglas Astronautics Co., Western Div., Santa Monica, Calif.

Simple Formulas for Unsteady Pressure on Slender Wedges and Cones in Hypersonic Flow

K. J. Orlik-Rückemann*
National Aeronautical Establishment, Ottawa, Canada

Inviscid surface pressure on slender wedges and cones performing small-amplitude pitching or plunging oscillation has been calculated by McIntosh,[1,2] using the hypersonic small-disturbance theory. Similar information but for slender wedges performing pitching oscillation with an amplitude of the order of the wedge semiangle has been obtained by Kuiken.[3,4] However, the results of all this work are not too readily available; McIntosh's results are in the form of graphs of the static and dynamic lift and pitching moment derivatives vs the inverse of the hypersonic similarity parameter K and also, for wedges only, in the form of an infinite series, whereas Kuiken's results are given as closed-form expressions, but containing functions of K which are only available in the form of a table. In the present Note simple formulas are presented with which the inviscid surface pressures at low frequencies in all the aforementioned cases can be rapidly calculated. It is also shown that for small amplitudes, the error introduced by omission of higher-order terms in frequency is generally less than 1% for reduced frequencies as high as 0.3.

Slender Wedge—Small Amplitude (Any γ)

Let us consider surface pressure on a wedge as the sum of a mean pressure $\bar{p}_m$ associated with the wedge semiangle θ_w and an unsteady oscillatory pressure $\bar{p}_{\text{osc}}$ caused by the oscillation of the wedge. The two pressure components may be obtained from the analysis of Ref. 1. Denoting by U and L the upper and the lower surface of the wedge, respectively, we have

$$\bar{p}_m = \bar{p}_\infty(2\gamma K^2 - \gamma + 1)/(\gamma + 1) \tag{1a}$$

$$[\bar{p}_{\text{osc}}]_{U,L} = \mp\bar{p}_\infty\gamma M_\infty{}^2\tau\bar{\alpha}e^{ikt}A \times \left\{F_1 + 2e^{-ikx}\sum_{n=1}^{\infty}(-\lambda)^n e^{ik\Gamma nx}F_2\right\} \tag{1b}$$

where $\bar{p}_\infty$ is the freestream pressure, γ is the specific heat ratio, M_∞ and U_∞ are the freestream Mach number and velocity, τ is the unperturbed shock wave angle, $\bar{\alpha}$ is the amplitude of oscillation, $k = \omega c/U_\infty$ is the reduced frequency based on the wedge chord c, $\bar{t} = tc/U_\infty$ is time, $\bar{x} = xc$ is the axial distance from the leading edge, and A, λ, and Γ are functions of K and γ as follows:

$$A = \{[2\gamma K^2 - \gamma + 1]/[(\gamma - 1)K^2 + 2]\}^{1/2}$$

$$\lambda = [(K^2 + 1)A - 2K^2]/[(K^2 + 1)A + 2K^2]$$

$$\Gamma = (A - 1)/(A + 1)$$

K is the hypersonic similarity parameter based on the unperturbed shock wave slope, that is, $K = M_\infty\tau$. For a wedge performing pitching oscillation around $x = x_0$, we have

$$F_1 = 1 + ik(x - x_0),\ F_2 = 1 + ik(\Gamma^n x - x_0)$$

whereas for a wedge performing plunging oscillation

$$F_1 = ik,\ F_2 = ik$$

Expanding the exponential functions in Eq. (1b), retaining only terms to the order of k^3, and performing the indicated summations, the unsteady oscillatory pressure on a wedge, which performs pitching oscillation $\theta = \theta_0 e^{i\omega\bar{t}} = \bar{\alpha}e^{ikt}$ around $x = x_0$ (where positive θ reduces the inclination of the upper surface to the flow), may be written, for $\theta \ll \tau$,

$$[\bar{p}_{\text{osc}}]_{U,L} = \mp\bar{p}_\infty\gamma M_\infty AK\{\theta[B_1 + xk^2(xB_4 + x_0B_5)] + \dot{\theta}[xB_2 + x_0B_3 + x^2k^2(xB_6 + x_0B_7)](c/U_\infty)\} \tag{2}$$

The corresponding expression for a wedge that performs plunging oscillation $h = h_0 e^{i\omega\bar{t}} = \bar{\alpha}e^{ikt}$ (where hc is displacement positive down) is, for $h \ll \tau$,

$$[\bar{p}_{\text{osc}}]_{U,L} = \pm\bar{p}_\infty\gamma M_\infty AK\{hxk^2B_5 + \dot{h}[B_3 + x^2k^2B_7](c/U_\infty)\} \tag{3}$$

It may be noted that Eq. (3) can be obtained directly from Eq. (2) by setting, in Eq. (2), $x_0 \gg 1$ (whereas $0 \leq x \leq 1$), $\theta = -h/x_0$, and $\dot{\theta} = -\dot{h}/x_0$.

Functions $B_1, B_2, \ldots, B_7$ depend only on K and γ and are

$$B_1 = 1 - 2C_0,\ B_2 = 1 + 2C_0 - 4C_1$$

$$B_3 = -1 + 2C_0 = -B_1,\ B_4 = C_0 - 4C_1 + 3C_2$$

$$B_5 = 2C_0 - 2C_1,\ B_6 = -\tfrac{1}{3}C_0 + 2C_1 - 3C_2 + \tfrac{4}{3}C_3 \tag{4}$$

$$B_7 = -C_0 + 2C_1 - C_2$$

where

$$C_n = \lambda\Gamma^n/(1 + \lambda\Gamma^n) \qquad (n = 0,1,2,3)$$

Table 1 Constants for Eq. (9)

Function	a	b	c	d	e
R, $\gamma = \frac{7}{5}$	2.6667	2.4794	1.3733	1.8144	−0.0204
S, $\gamma = \frac{7}{5}$	−2.0000	−1.8055	0.0001	0.7599	−0.1290
R, $\gamma = \frac{5}{3}$	2.2856	2.5128	1.3700	1.4511	0.0163
S, $\gamma = \frac{5}{3}$	−2.0000	0.1725	0.0020	−0.2863	0.0165

Received July 22, 1969. The author is indebted to S. C. McIntosh Jr. of Stanford University for making available the unpublished numerical results of his analysis.

* Head, Unsteady Aerodynamics Laboratory. Associate Fellow AIAA.